Contribution from the Department of Chemistry,
Stanford University, Stanford, California 94305

Coordination Chemistry of NH_3 on ZnO(0001) and CuCl(111) Surfaces: σ-Bonding Interactions with d^{10} Metal Ion Sites

Jianyi Lin, Paul M. Jones, Michael D. Lowery, Robert R. Gay, Susan L. Cohen, and Edward I. Solomon*

Received August 1, 1991

NH_3 adsorption on ZnO(0001) and CuCl(111) surfaces has been studied using a combination of ultraviolet photoelectron spectroscopy (UPS), X-ray photoelectron spectroscopy (XPS), and self-consistent-field-Xα-scattered wave (SCF-Xα-SW) electronic structure calculations. Both surfaces consist of coordinatively unsaturated tetrahedral d^{10} metal ion sites with their open coordination positions normal to the surface. Physisorption is dominant on both surfaces at high NH_3 coverages. The NH_3 $3a_1$-$1e$ orbital energy splitting at high ammonia coverages is 5.4 eV, which is the same as for gas-phase NH_3. The physisorbed nitrogen 1s level was found at 405.0 eV for NH_3/ZnO(0001) and at 405.8 eV for the NH_3/CuCl(111) surface. At low coverages, chemisorbed molecular NH_3 is found to dominate on both surfaces. The NH_3 $3a_1$, $1e$ and nitrogen 1s ionization energies were observed at 12.5, 16.5, and 403.0 eV below the vacuum level for ZnO(0001) and at 12.5, 15.5, and 403.5 eV for CuCl(111). The $3a_1$-$1e$ splitting decreases to a greater extent for chemisorption to Cu(I) (2.4 eV) relative to Zn(II) (1.4 eV). Both surfaces show a decrease in the surface dipole moment upon NH_3 adsorption (-1.4 eV for ZnO(0001) versus -1.3 eV for CuCl(111)), which indicates that charge is transferred from the NH_3 $3a_1$ molecular orbital to the surface. This is consistent with the net positive charge gained by the nitrogen atom as found from XPS core studies; the nitrogen atom donates 0.06 of a unit charge when coordinated to Zn(0001) and 0.09 for CuCl(111). Heat of adsorption measurements for NH_3 chemisorption find $\Delta H_0 = 28 \pm 3$ kcal/mol for ZnO(0001) and 24 ■ 3 kcal/mol for CuCl(111). The ionic contribution for NH_3 binding was estimated to be 17 and 9 kcal/mole for ZnO and CuCl, respectively; thus, the covalent contribution to bonding is larger for Cu(I). SCF-Xα-SW calculations have been used to verify assignments in the UV photoelectron spectrum. The Xα calculations also show that ammonia has a greater covalent interaction with Cu(I) than with Zn(II) sites. Examination of the change in the atomic charge distribution summed over all valence levels induced upon NH_3 binding shows that there is a net increase of 3.2% 4s and 13.2% 4p character for Cu(I), while Zn(II) has a net loss of 0.87% 4s and a small increase of 5.2% 4p character. The increased covalency for NH_3 σ bonding to Cu(I) relative to Zn(II) is discussed in terms of greater orbital overlap due to its reduced effective nuclear charge.

I. Introduction

The adsorption of ammonia on metal surfaces has been extensively studied[1-27] due to its importance as a reactant or product in transition-metal catalysis. However, less attention has been paid to the adsorption of ammonia on metal oxide surfaces although some ammoxidation reactions involve metal oxide catalysts.[28,29]

Our previous investigation of the adsorption of CO by the d^{10} metal ion surface sites on CuCl and ZnO indicates that the covalent bonding of CO to Zn(II) is weak and results mainly from σ donation,[30] whereas the bonding of CO to Cu(I) is stronger and has contributions from both σ donation and π back-bonding.[31] The lowest unoccupied molecular orbital of CO, $2\pi^*$, is located 1.5 eV above the vacuum level for gas-phase CO and between the vacuum and Fermi levels for adsorbed CO.[31] π back-bonding is negligible in CO/ZnO due to the unavailability of the deep-lying Zn 3d orbitals for back-donation (16.3 eV below the vacuum level). π back-bonding occurs in CO/CuCl on the basis of observations[31] of an intense core-level satellite peak and a CO binding induced shift of the Cu $3d_\pi$ levels to deeper binding energy. This results from the availability of the low-lying Cu(I) d band at ~7 eV. These differences in π bonding complicate a comparison of the relative strengths of CO σ-bond interactions with these two d^{10} metal ions.

In NH_3 the lowest unoccupied molecular orbitals, $4a_1$ and $2e$, are Rydberg states 5.5 and 7.0 eV above the vacuum level.[32] NH_3 bonding to metal ion sites is generally treated as involving a dominant σ interaction with no π back-bonding. Consequently, NH_3 can be used as a probe of σ donation to Cu(I) and Zn(II) ions.

ZnO(0001) and CuCl(111) have similar surface structures. Crystalline ZnO adopts the wurtzite structure, and its (0001) surface can be viewed as a plane of C_{3v}-distorted tetrahedral Zn(II) ions with coordinatively unsaturated directions normal to the surface. In CuCl crystals, copper and chlorine ions are combined in the zinc-blende arrangement, which produces three-coordinate, unsaturated C_{3v} Cu(I) sites on the (111) surface. Aside from the similar atomic arrangement, the electronic structure of the two

(1) Lambert, R. M.; Bridge, M. E. In *The Chemical Physics of Solid Surfaces and Heterogeneous Catalysis*; King, D. A., Woodruff, D. P., Eds.; Elsevier: Amsterdam, 1983; Vol. 3B, p 59.
(2) Tochihara, H.; Rocker, G.; Redding, J. D.; Yates, J. T., Jr.; Martin, R. M.; Metiu, H. *Surf. Sci.* **1986**, *176*, 1.
(3) Grunze, M.; Golze, M.; Driscoll, R. K.; Dowben, P. A. *J. Vac. Sci. Technol.* **1981**, *18*, 611.
(4) Grunze, M.; Dowben, P. A.; Brundle, C. R. *Surf. Sci.* **1983**, *128*, 311.
(5) Seabury, C. W.; Rhodin, T. N.; Purtell, R. J.; Merrill, R. P. *Surf. Sci.* **1980**, *93*, 117.
(6) Lee, L.; Arias, J.; Hanrahan, C.; Martin, R. M.; Metiu, H. *Surf. Sci.* **1986**, *165*, L95.
(7) Jacobi, K.; Jensen, E. S.; Rhodin, T. N.; Merrill, R. P. *Surf. Sci.* **1981**, *108*, 397.
(8) Hüttinger, M.; Küppers, J. *Surf. Sci.* **1983**, *130*, L277.
(9) Egelhoff, W. F.; Linnett, J. W.; Perry, D. I.. *Faraday Disc. Chem. Soc.* **1975**, *60*, 127.
(10) Lanzillotto, A.; Dresser, M. J.; Alvey, M. D.; Yates, J. T., Jr. *Surf. Sci.* **1987**, *191*, 15.
(11) Benndorf, C.; Madey, T. E.; Johnson, A. L. *Surf. Sci.* **1987**, *187*, 434.
(12) Weiss, M.; Ertl, G.; Nitschke, F. *Appl. Surf. Sci.* **1979**, *2*, 614.
(13) Grunze, M.; Bozso, F.; Ertl, G.; Weiss, M. *Appl. Surf. Sci.* **1978**, *1*, 241.
(14) Kishi, K.; Roberts, M. W. *Surf. Sci.* **1977**, *62*, 252.
(15) Grunze, M. *Surf. Sci.* **1979**, *81*, 603.
(16) Grunze, M.; Brundle, C. R.; Tomanek, D. *Surf. Sci.* **1982**, *119*, 133.
(17) Reed, A. P. C.; Lambert, R. M. *J. Phys. Chem.* **1984**, *88*, 1954.
(18) Sexton, B. A.; Mitchell, G. E. *Surf. Sci.* **1980**, *99*, 523.
(19) Fisher, G. B. *Chem. Phys. Lett.* **1981**, *79*, 452.
(20) Sexton, B. A.; Mitchell, G. E. *Surf. Sci.* **1980**, *99*, 539.
(21) Biwer, B. M.; Bernasek, S. L. *Surf. Sci.* **1986**, *167*, 207.
(22) Gland, J. L.; Sexton, B. A.; Mitchell, G. E. *Surf. Sci.* **1982**, *115*, 623.
(23) Sesselmann, W.; Woratschek, B.; Ertl, G.; Küppers, J.; Haberland, H. *Surf. Sci.* **1984**, *146*, 17.
(24) Kubler, L.; Hill, E. K.; Bolmont, D.; Gewinner, G. *Surf. Sci.* **1987**, *183*, 503.
(25) Fukuda, Y.; Rabalais, J. W. *J. Electron Spectrosc. Relat. Phenom.* **1982**, *25*, 237.
(26) Danielson, L. R.; Dresser, M. J.; Donaldson, E. E.; Dickinson, J. T. *Surf. Sci.* **1978**, *71*, 599.
(27) Kung, H. H. *Transition Metal Oxides: Surface Chemistry and Catalysis*; Elsevier: Amsterdam, 1989; p 63.
(28) Hucknall, D. J. *Selective Oxidation of Hydrocarbons*; Academic Press: London, 1974; p 23.
(29) Cavani, F.; Centi, G.; Nieto, J. L.; Pinelli, D.; Trifiro, F. In *Heterogeneous Catalysis and Fine Chemicals*; Guisnet, M., Barrault, J., Bouchoule, C., Duprez, D., Montassier, C., Perot, G., Eds.; Elsevier: Amsterdam, 1988; p 345.
(30) Gay, R. R.; Nodine, M. H.; Henrich, V. E.; Zeiger, H. J.; Solomon, E. I. *J. Am. Chem. Soc.* **1980**, *102*, 6752 and references therein.
(31) Lin, J.; Jones, P. M.; Guckert, J. A.; Solomon, E. I. *J. Am. Chem. Soc.* **1991**, *113*, 8312.
(32) Rodriguez, J. A.; Campbell, C. T. *Surf. Sci.* **1988**, *194*, 475.

0020-1669/92/1331-0686$03.00/0

surfaces is very different. In ZnO, as mentioned above, the metal 3d band is centered at 16.3 eV below the vacuum level and well below the oxygen 2p levels (~9–14 eV) and the empty 4s level (5.2 eV below the vacuum level). In CuCl, the copper 3d, the chlorine 3p and the empty copper 4s levels are found at 7, 11, and 3 eV below the vacuum level, respectively. These differences in electronic structures are expected to result in different bonding descriptions for the isoelectronic metal ion sites in the NH_3/ZnO(0001) and NH_3/CuCl(111) systems. It should be noted that the dominant σ-bonding interaction involves the HOMO, NH_3 $3a_1$ level (at ~11.0 eV) with the unoccupied 4s and 4p levels on the metal ion. The metal d band can also interact with the NH_3 $3a_1$ level and perturb its energy (Cu 3d stabilizing and Zn 3d destabilizing the $3a_1$ orbital). However, as the metal d manifold is filled, these interactions do not contribute to net bonding of NH_3 to the metal ion surface sites.

In this study a combination of UPS, XPS, and SCF–Xα–SW electronic structure calculations has been used to investigate the adsorption of NH_3 on the ZnO(0001) and CuCl(111) surfaces. In section III.A1, UPS was used to study NH_3 adsorption on the ZnO(0001) surface. Using surface coverage and sample temperature as controlling parameters, both chemisorbed and physisorbed NH_3 species were found to be present on the surface. Additionally, the intensity of the NH_3-derived peak in the He II UP spectrum was measured as a function of temperature and pressure to determine the heat of adsorption of NH_3 to this surface. In section III.A2, He I UPS was used to find the surface dipole moment change upon NH_3 absorption. Section III.A3 presents the results of the nitrogen 1s core level data on NH_3/ZnO(0001) collected using synchrotron radiation. Parallel experiments were performed on NH_3/CuCl(111), and the results are presented in section III.B. The results of the SCF–Xα–SW calculations for both systems are presented in section III.C. These calculations reproduce the experimental UPS data for both surface sites and provide a description of NH_3 bonding to these d^{10} metal ion sites. The bonding differences between Cu(I) and Zn(II) are summarized and discussed in section IV.

II. Experimental Section

The CuCl(111) surface was prepared by cutting a 1-mm plate from a single crystal of CuCl. The (111) face was oriented to within ±1° by Laue backscattering. The surface was then polished with successive sizes of alumina grit (to 0.1 μm) until no pits were visible by microscopic inspection. The surface was then chemically etched with a mixture of concentrated hydrochloric acid and anhydrous ethanol followed by an acetone rinse. Surface cleaning was completed in UHV by a series of sputter/anneal cycles. Ion beams with energies greater than 1.1 keV were found to preferentially sputter chlorine; therefore, argon ion sputtering was performed at energies between 900 and 1000 eV with an ion flux density of 1–4 mA/cm^2. The sample temperature was maintained at approximately 350 K throughout the sputter and anneal process.

The surface cleanliness, chemical stoichiometry, and metal oxidation state were monitored with XPS and UPS. Electron beam induced Auger spectroscopy was not used in the study of CuCl due to the high probability of surface damage from the electron beam, as was observed by scanning Auger microscope experiments. A clean surface produced XPS spectra with no photoemission features other than those of Cu and Cl. The atomic ratio of copper versus chlorine was estimated from the intensities of the Cu $2p_{3/2}$ and Cl 2p bands. Since the Cu 2p level lies at the same binding energy for both Cu(I) and Cu(0),[33] the oxidation state of copper was determined using the X-ray-induced Cu $L_3M_{4,5}M_{4,5}$ Auger peak. Prolonged X-ray irradiation at room temperatures was found to result in changes in the Cu/Cl atomic ratio and was avoided.

Surface order was checked using low-energy electron diffraction (LEED). LEED gave the expected hexagonal pattern for the clean surface, indicating that no symmetry changing surface reconstruction occurs. LEED patterns were observed only when the energy of the incident electron beam was higher than a threshold value, which is the secondary emission crossover.[34]

ZnO samples were also 1-mm-thick plates cut from a single crystal. The sample was oriented within ±1° of the (0001) direction by Laue backscattering, polished with alumina grit, and etched with a 5% HCl solution. Argon ion sputtering was performed at successive accelerating potentials of 1000, 500, and 250 V at 720 K in UHV, followed by annealing at this temperature. ZnO sample cleanliness was checked with Auger spectroscopy.

All experiments on the CuCl(111) surface were carried out in a Vacuum Generators ESCALAB MK II instrument equipped with XPS, UPS, AES, and LEED capabilities using a hemispherical electron energy analyzer (150° spherical sector of 150-mm radius). A discharge lamp produced He II (40.8 eV) and He I (21.2 eV) photons propagating at an angle 15° off the vertical. A Mg Kα (1253.6 eV) X-ray source was used for core level studies. The sample was heated and cooled in situ, and the sample temperature was measured using a chromel–alumel thermocouple attached to the sample holder. All gases used were of research purity (Matheson, 99.99%). NH_3 was introduced into the experimental chamber from a separate UHV line through a Varian leak valve. The ammonia pressure and doses were monitored using an ionization gauge. The base pressure of the system was maintained at ~5 × 10^{-11} mbar (2 × 10^{-10} mbar with the He resonance lamp in operation). All adsorption experiments were carried out at low temperatures. CuCl is a p-type semiconductor with a wide band gap of 3.4 eV.[35] At low temperatures charging caused by photoemission became severe. An electron flood gun was employed (operated at 1.5–2.0 V and 2.0 A) in order to compensate for charging. Care was taken to avoid distorting the overall spectral shape at low temperatures by comparing to line shapes observed at high temperatures. Nevertheless, some sample charging did occur and peak energies were corrected using the chloride 2p core and chlorine 3p valence levels as references.

Experiments employing synchrotron radiation as a photon source were performed on beam line III-1 at the Stanford Synchrotron Radiation Laboratory (SSRL) under dedicated conditions using a grasshopper monochromator. The UHV system used for these experiments was a Perkin-Elmer Ultek chamber with a double-pass cylindrical mirror analyzer (CMA) and ion sputtering gun. The CMA accepts a 6° cone of electrons with a half-angle of 42.5° off the CMA axis. For the core-level PES, wide analyzer slits and large pass energies were utilized, which increase the signal-to-noise ratio but limit the resolution to 1.3 eV. Ammonia exposures were performed at 130 K with the NH_3 pressure held between 1 × 10^{-8} and 5 × 10^{-7} mbar for an appropriate time. This was followed by evacuation of the chamber and data acquisition. UPS studies on ZnO utilizing a resonance photon source were taken in a Physical Electronics ion-pumped UHV system equipped with CMA and using an energy resolution of approximately 0.2 eV. All spectra were signal-averaged until a satisfactory signal-to-noise ratio had been established.

The 1982 QCPE release[36] of the SCF–Xα–SW program was used for the electronic structure calculations. The code was implemented using a MIPS Fortran compiler on a Digital 3100 computer system. Lacking specific structural data for NH_3 bound to either ZnO(0001) or CuCl(111), the ammonia molecule was assumed to interact with the metal oxide (chloride) surface via the nitrogen atom in an eclipsed conformation. This results in a model having C_{3v} site symmetry. The ammonia–metal distance was estimated from known crystal structures of ammine-coordinated Zn(II) and Cu(I) compounds.[37–39] To render the surface site tractable for the electronic structure calculations, the metal oxide (chloride) lattice was truncated to include the metal and only its immediate coordination sphere. The molecular geometry and the relevant parameters used in the SCF–Xα–SW calculations are collected in Table I.

The atomic exchange parameters, α, were taken from Schwarz,[40] and the valence-electron-weighted average of the atomic α values was used

(33) Wagner, C. D.; Riggs, W. M.; Davis, L. E.; Moulder, J. F.; Muilenberg, G. E. *Handbook of X-ray Photoelectron Spectroscopy*, 2nd ed.; Perkin-Elmer: Norwalk, CT, 1979, p 87.
(34) French, T. M.; Somorjai, G. A. *J. Phys. Chem.* **1970**, *74*, 2489.
(35) Nikitine, S. *Prog. Semicond.* **1962**, *6*, 271.
(36) For reviews of the SCF–Xα–SW method, see: (a) Slater, J. C. *Adv. Quantum Chem.* **1972**, *6*, 1. (b) Johnson, K. H. *Adv. Quantum Chem.* **1973**, *7*, 143. (c) Case, D. A. *Annu. Rev. Phys. Chem.* **1982**, *33*, 151. (d) Johnson, K. H. *Annu. Rev. Phys. Chem.* **1975**, *26*, 39. (e) Connolly, J. W. D. In *Semiempirical Methods of Electronic Structure Calculation, Part A: Techniques*; Segal, G. A., Ed.; Plenum: New York, 1977; p 105. (f) Johnson, K. H.; Norman, J. G., Jr.; Connolly, J. W. D. In *Computational Methods for Large Molecules and Localized States in Solids*; Herman, F.; McLean, A. D.; Nesbet, R. K., Eds.; Plenum: New York, 1973; p 161. (g) Cook, M. Ph.D. Dissertation, Harvard University, Boston, MA, 1981.
(37) Brown, C. J.; Cook, D. S.; Sengier, L. *Acta Crystallogr., Sect. C* **1987**, *43*, 2332.
(38) Brown, C. J.; Cook, D. S.; Sengier, L. *Acta Crystallogr., Sect. C* **1985**, *41*, 718.
(39) Baenziger, N. C.; Modak, S. L.; Fox, C. L., Jr. *Acta Crystallogr., Sect. C* **1983**, *39*, 1620.
(40) Schwarz, K. *Phys. Rev. B* **1972**, *5*, 2466.

Table I. Parameters Used in the SCF-Xα-SW Program[a]

atom	x	y	z	α	sphere radius
outer sphere	0.0000	0.0000	0.0000	0.726 41	6.7220
Cu	0.0000	0.0000	0.0000	0.706 97	2.4500
Cl	4.1691	0.0000	−1.0945	0.723 25	2.4000
Cl	−2.0846	3.6105	−1.0945	0.723 25	2.4000
Cl	−2.0846	−3.6105	−1.0945	0.723 25	2.4000
N	0.0000	0.0000	4.2912	0.751 97	1.9000
H	1.7958	0.0000	4.9262	0.777 25	1.0000
H	−0.8980	1.5552	4.9262	0.777 25	1.0000
H	−0.8980	−1.5552	4.9262	0.777 25	1.0000
outer sphere	0.0000	0.0000	0.0000	0.736 92	5.6417
Zn	0.0000	0.0000	0.0000	0.706 73	2.3295
O	3.5271	0.0000	−1.2490	0.744 47	2.0000
O	−1.7635	3.0545	−1.2490	0.744 47	2.0000
O	−1.7635	−3.0545	−1.2490	0.744 47	2.0000
N	0.0000	0.0000	3.8551	0.751 97	1.9000
H	1.7958	0.0000	4.4900	0.777 25	1.0000
H	−0.8980	1.5552	4.4900	0.777 25	1.0000
H	−0.8980	−1.5552	4.4900	0.777 25	1.0000

[a] All distances are in bohrs (1 bohr = 0.529 177 Å).

for the inner- and outer-sphere α values. A Watson sphere was used for all ionic species and its radius was 0.1 bohr greater than the outer-sphere radius. Calculations were considered converged when the largest deviation of the atomic potentials between SCF cycles was less than 10^{-4}. This was usually achieved within 250–350 SCF iterations. Initial calculations were performed with atomic sphere radii chosen using the Norman[41] criteria with the outer-sphere radius overlapping the outermost atomic sphere by 0.1 bohr. The accuracy of the wave functions obtained using the Norman radii were evaluated by comparing the experimental UV photoelectron spectra (UPS) to that calculated by the SCF-Xα-SW method using the Slater transition-state[42] formalism. The transition-state energies calculated for both surface models using the Norman radii were not in reasonable agreement with the observed UPS data. The NH_3 $3a_1$–1e splitting was calculated to be 7.509 eV for $[CuCl_3NH_3]^{2-}$ and 9.337 eV for $[ZnO_3NH_3]^{4-}$; the $3a_1$–1e splitting calculated for gaseous NH_3 was 6.527 eV. The experimental UPS splitting for ammonia is 5.4 eV in the gas phase, ~3.1 eV for NH_3/CuCl(111), and ~4.1 eV for NH_3/ZnO(0001) (vide infra). Similar problems[43] have been encountered when using the Norman criteria, and it has been shown that the Norman radii overestimate ligand covalency in transition-metal systems.

To compensate for this deficiency, the atomic sphere radii were systematically adjusted to give better agreement with the experimental data. For $[CuCl_3NH_3]^{2-}$, the copper sphere radius was held fixed at 2.4500 bohr (approximately its Norman value), and the chlorine, nitrogen, and hydrogen sphere radii were adjusted. The hydrogen atom sphere radii were fixed at 1.0000 bohr, as suggested by Herman et al.[44] The nitrogen radius was increased from 1.6977 to 1.9000 bohr in accordance with the optimal radius found by Gewirth et al.[43c] for the ammonia molecule in a plastocyanin model complex. The chlorine radius was reduced from 2.7673 to 2.4000 bohr. This was done to increase the energy splitting between the chlorine 3p and copper 3d bands (as observed experimentally). These radii were found to greatly improve the fit to the experimental data (vide infra; see Figures 1 and 6). To allow for direct comparisons, the same set of radii were used in the $[ZnO_3NH_3]^{4-}$ model, with the oxygen radius also being reduced from its Norman value as was done for chlorine (by approximately the same amount). The optimized atomic sphere radii thus obtained are given in Table I. The NH_3 $3a_1$–1e orbital splitting for the optimal sphere radii was found to be 5.52 eV for $[CuCl_3NH_3]^{2-}$ and 6.14 eV for $[ZnO_3NH_3]^{4-}$.

SCF-Xα-SW calculations were also performed for the surface sites in the absence of coordinated ammonia, i.e. $[ZnO_3]^{4-}$ and $[CuCl_3]^{2-}$ (ground-state energies and valence-charge distributions are available in the supplementary material). These calculations were used to quantify the changes which occur upon ammonia binding. The sphere radii used for the clean surface model (including the outer and Watson spheres) were identical to those used when ammonia was bound.

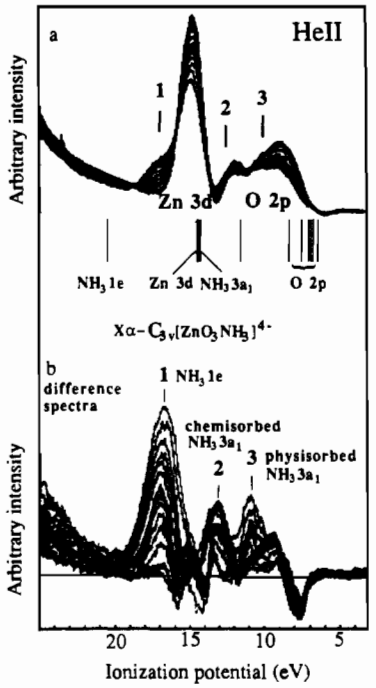

Figure 1. He II valence band spectra of NH_3 on ZnO(0001). Part a shows data for the ZnO(0001) surface exposed to a 1×10^{-6} mbar NH_3 ambient as a function of temperature (110–450 K). The spectra have been aligned to the Zn 3d band. Part b gives the NH_3-covered minus clean ZnO(0001) difference spectra at a variety of temperatures. The calculated SCF-Xα-SW ionization energies for $[ZnO_3NH_3]^{4-}$ are included below the experimental UPS data for comparison.

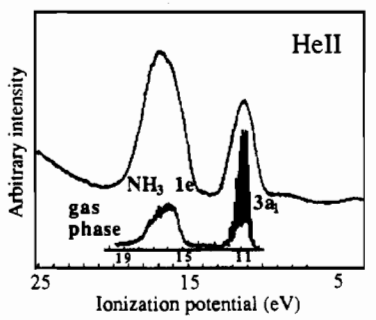

Figure 2. He II photoemission spectrum of condensed NH_3 on ZnO(0001). The spectrum was recorded with the surface in equilibrium with a 1×10^{-6} mbar NH_3 ambient at 90 K. The He I spectrum of gas-phase NH_3 is included for comparison (from ref 45).

III. Results and Analysis

A. PES Study of NH_3/ZnO(0001). 1. Valence Band Photoemission and Heat of Adsorption. Ultraviolet photoemission spectra for the ZnO(0001) surface exposed to an ambient pressure of NH_3 (1×10^{-6} mbar) at temperatures of 110–450 K are shown in part a of Figure 1. Note that the energy levels reported for ZnO and CuCl are referenced to the vacuum rather than the Fermi level in order to facilitate their comparison due to the poor conductivity of CuCl. The UPS spectrum of the clean ZnO(0001) surface is composed of two major bands: the zinc 3d band at 14–17 eV below the vacuum level and the oxygen 2p band at 9–14 eV. At low NH_3 coverages, two new bands at 16.5 and 12.5 eV (labeled 1 and 2 in Figure 1) emerge. These bands are more evident in the difference spectra shown in part b in Figure 1. On the basis of SCF-Xα-SW calculations and the band positions observed in the UPS spectrum of condensed NH_3 shown in Figure 2 (vide infra), these peaks are assigned as the 1e and $3a_1$ states of chemisorbed NH_3, respectively. The $3a_1$–1e energy splitting for chemisorbed NH_3 is 4 eV, which corresponds to a stabilization of 1.4 eV for the NH_3 $3a_1$ orbital relative to its value in the gas

(41) Norman, J. G. *Mol. Phys.* **1976**, *31*, 1191.
(42) Slater, J. C. *The Self-Consistent Field for Molecules and Solids: Quantum Theory of Molecules and Solids*; McGraw-Hill: New York, 1974; Vol IV.
(43) (a) Gewirth, A. A.; Cohen, S. L.; Schugar, H. J.; Solomon, E. I. *Inorg. Chem.* **1987**, *26*, 1133. (b) Didziulis, S. V.; Cohen, S. L.; Gewirth, A. A.; Solomon, E. I. *J. Am. Chem. Soc.* **1988**, *110*, 250. (c) Gewirth, A. A.; Solomon, E. I. *J. Am. Chem. Soc.* **1988**, *110*, 3811.
(44) Herman, F.; Williams, A. R.; Johnson, K. H. *J. Chem. Phys.* **1974**, *61*, 3508.

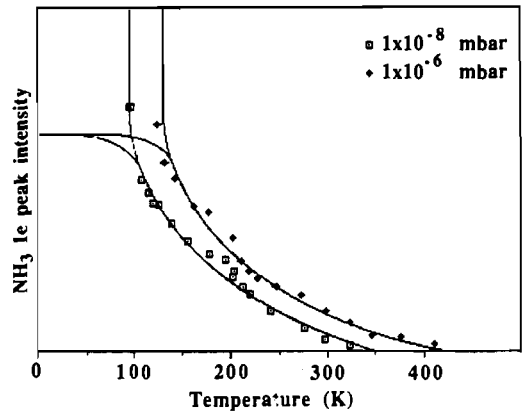

Figure 3. Variation in the equilibrium coverage of NH_3 on ZnO(0001) surface as a function of temperature and pressures as measured by the NH_3 1e intensity. The data have been fit to a Temkin isobar given by $\theta/(1-\theta) = K\exp[\Delta H_0(1-\alpha\theta)/RT]$, with $a \simeq 0.6$ and $K \simeq 0.5 \times 10^{-14}$ (see ref 30). The fit to the data gives the heat of adsorption for chemisorbed ammonia, ΔH_0, of 28 ± 3 kcal/mol. The high NH_3 coverage data (i.e. $<\sim 140$ K) are fit to a second isobar giving a heat of adsorption for physisorbed ammonia of $\sim 6 \pm 3$ kcal/mol.

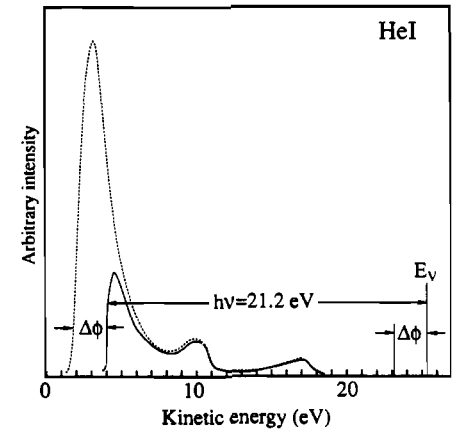

Figure 4. He I UPS estimate of the work function change of the ZnO-(11$\bar{2}$0) surface upon NH_3 adsorption. The solid line is the He I UPS spectrum for the clean ZnO(11$\bar{2}$0) surface, and the dashed line is for the ZnO(11$\bar{2}$0) surface in equilibrium with a 1×10^{-6} mbar ambient of NH_3 at 110 K. The spectra are aligned to the Zn 3d band to correct for changes in band bending. The 2.1-eV shift to lower kinetic energy in the onset of the secondary electron tail gives the surface dipole moment change ($\Delta\phi$) upon NH_3 adsorption.

phase.[45-48] The observed chemical shift of the $3a_1$ orbital confirms that the chemisorbed NH_3 molecule is bound to the Zn(II) ion via the nitrogen atom. At higher NH_3 coverages, physisorbed ammonia begins to accumulate, as is evident by the appearance of and increase in intensity of the band at ~11.1 eV (peak 3 in Figure 1). Figure 2 shows the UPS spectrum of the ZnO surface collected at low temperature (~90 K) and long exposure times to 1×10^{-6} mbar NH_3 (which is greater than the equilibrium vapor pressure of NH_3 at 90 K, $<1 \times 10^{-8}$ mbar[49]). These conditions lead to multilayer physisorption and ultimately attenuate all the UPS features attributable to the ZnO substrate. The high NH_3 coverage limit exhibits only two peaks with an energy splitting of 5.4 eV, the same value as observed for gaseous ammonia (insert in Figure 2). These data confirm the assignment of band 3 in Figure 1 as arising from physisorbed ammonia, even at moderately low NH_3 concentrations. This implies that ammonia clusters on the ZnO surface before chemisorption is complete.

The intensity of the NH_3 1e peak depends on the surface temperature and the equilibrium NH_3 pressure. It can be used to monitor the surface coverage to determine the heat of adsorption of NH_3 on ZnO(0001). Figure 3 presents a plot of the intensity of the 1e peak as a function of sample temperature and NH_3 pressure. The heat of adsorption at a given NH_3 coverage, $\Delta H(\theta)$, can be determined using the Clausius–Clapeyron equation:[50]

$$[\Delta(\ln P)/\Delta(1/T)]_\theta = -\Delta H_{ads}/R \quad (1)$$

A linear decrease of $\Delta H(\theta)$ with increasing NH_3 coverage is found from the data in Figure 3. For a well-formed single-crystal surface this decrease should be due to repulsive dipole–dipole interactions between NH_3 molecules and can be described by the Temkin isobar expression:[51]

$$\Delta H(\theta) = \Delta H_0(1-\alpha\theta) \quad (2)$$

Here α is a constant and ΔH_0 is the heat of adsorption at zero coverage. From the NH_3/ZnO(0001) data in Figure 3, the heat of adsorption extrapolated to zero NH_3 coverage is found to be 28 ± 3 kcal/mol. The low-temperature data correspond to physisorbed species and are fit to another set of isobars giving a heat of adsorption of 6 ± 3 kcal/mol (which is close to the 5.6 kcal/mol heat of evaporation of NH_3[49]).

2. NH_3–ZnO Surface Dipole Moment. Figure 4 presents He I spectra of clean and NH_3 covered ZnO surfaces. Note that in Figure 4 we present results obtained for the NH_3/ZnO(11$\bar{2}$0) surface, rather than the NH_3/ZnO(0001) surface, because the clean (11$\bar{2}$0) surface is known to be more stable than the (0001) surface (for which zinc ions are found to relax into the surface)[30] and is less likely to undergo an adsorbate-induced surface reconstruction which may contribute to the total change in the surface dipole moment. In Figure 4 the onset of the secondary electron tail corresponds to electrons with zero kinetic energy. Therefore, the vacuum level, E_v, is 21.2 eV (the He I photon energy) above this onset. The shift in the electron tail upon NH_3 adsorption represents a shift in the vacuum level relative to a fixed Fermi level and gives the work function change.

For semiconductors, this shift in the surface work function ($\Delta\Phi$) has contributions from the change in the surface dipole moment ($\Delta\Phi_{dipole}$) and from the change in band bending ($\Delta\Phi_{bb}$). Charge separation results in the bending of the valence and conduction bands near the surface relative to their values in the bulk lattice. n-type semiconductors shift the bands to more positive energies, while p-type semiconductors deepen the band energy near the surface. ZnO is an extrinsic n-type semiconductor,[52] where the presence of zinc atoms in the lattice results in donor levels located just below the bottom of the conduction band. For upward band bending the total work function change is given by[53]

$$\Delta\Phi = \Delta\Phi_{dipole} + \Delta\Phi_{bb} \quad (3)$$

The change in the band bending for NH_3 absorption on ZnO can be determined from the valence band peak shift provided that the shape of the valence band does not change significantly with adsorption. In Figure 4, changes due to band bending are corrected by aligning the Zn 3d band of the NH_3 covered surface with that of the clean surface. The energy shift of the low kinetic energy limit of the secondary electron tail gives the change in the surface dipole moment. A 2.1 ± 0.1 eV decrease in the surface dipole moment is determined for the NH_3/ZnO(11$\bar{2}$0) surface[54]

(45) Turner, D. W.; Baker, C.; Baker, A. D.; Brundle, C. R. *Molecular Photoelectron Spectroscopy*; Wiley-Interscience: London, 1970, p 364.
(46) Campbell, M. J.; Liesegang, J.; Riley, J. D.; Leckey, R. C. G.; Jenkin, J. G. *J. Electron Spectrosc. Relat. Phenom.* **1979**, *15*, 83.
(47) Allison, D. A.; Cavell, R. G. *J. Chem. Phys.* **1978**, *68*, 593.
(48) Brion, C. E.; Hamnett, A.; Wight, G. R.; van der Wiel, M. J. *J. Electron Spectrosc. Relat. Phenom.* **1977**, *12*, 323.
(49) Honig, R. E.; Hook, H. O. *RCA Rev.* **1960**, *21*, 360.
(50) Farrington, R. A.; Daniels, A. *Physical Chemistry*, 5th ed.; John Wiley: New York, 1979; p 98.
(51) Hayward, D. O.; Trapnell, B. M. W. *Chemisorption*, 2nd ed.; Butterworths: Washington, DC, 1964; p 218.
(52) Bond, G. C. *Heterogeneous Catalysis: Principles and Applications*, 2nd ed.; Clarendon Press: Oxford, England, 1987; p 39.
(53) Ertl, G.; Gerischer, H. In *Physical Chemistry An Advanced Treatise*; Henderson, D., Wilhelm, J., Eds.; Academic Press: New York, 1976; Vol. X, p 371.

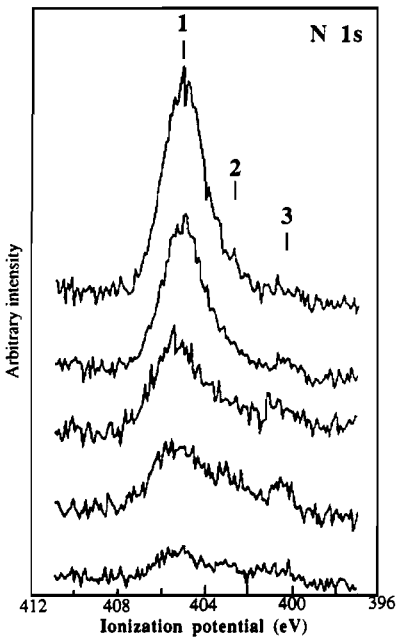

Figure 5. Nitrogen 1s photoelectron spectra of NH_3 adsorbed on the ZnO(0001) surface as a function of increasing exposure (from bottom to top) at 130 K. Exposures were controlled by maintaining the NH_3 pressure between 1×10^{-8} and 5×10^{-7} mbar and varying the exposure time. The spectra were collected with synchrotron radiation at $h\nu = 495$ eV. The energy of the peak maxima were determined by Gaussian/Lorentzian fit of the spectra.

(at 110 K and 1×10^{-6} mbar). The surface dipole moment caused by adsorption, μ, can be determined using the Helmholtz equation[55]

$$\Delta\Phi_{dipole} = 4\pi c_s \theta \mu \cos\beta \qquad (4)$$

where c_s is the number of surface sites per cm^2, θ is the fractional coverage of the surface (i.e. 0.5 of a monolayer coverage estimated from the He II thermodynamic studies of the adsorbate interaction[56]), and β is the angle between the Zn–N axis and the surface normal (i.e. $\beta = 35°$ assuming that the NH_3 molecule is bound to the Zn ion along the coordinatively unsaturated orientation of the adsorption site on Zn(11$\bar{2}$0)). This gives a value for the apparent surface dipole moment of $\mu = 2.0$ D negative side down. This apparent dipole moment would result from charge transferred from the adsorbed NH_3 to the substrate. NH_3 has a large dipole moment of 1.47 D in the gas phase. Binding to the surface via its nitrogen atom should result in a significant decrease in the surface dipole moment. In addition, adsorption can change the substrate internal dipole moment, complicating the analysis of the work function data. Assuming that both the adsorbed NH_3 molecule and the substrate internal dipole moment do not change upon binding, the extra surface dipole moment resulting from net negative charge transfer to the surface is 0.53 D. The net charge transferred to the substrate is given by $q = \mu/L = 0.05$, where L is the distance between the Zn(II) ion and the midpoint of the NH_3 dipole, estimated to be 2.3 Å). The XPS nitrogen 1s chemical shift is a more direct probe of net charge transfer from the nitrogen and is considered below.

3. Nitrogen 1s Core Level and Effective Atomic Charge. Nitrogen 1s photoemission spectra of NH_3 on ZnO(0001) are shown in Figure 5. An input photon energy of 495 eV (near the nitrogen 1s threshold) is used here because the nitrogen 1s photoionization cross section is a factor of 10 higher at this photon energy than at $h\nu = 1254$ eV (Mg Kα). Peak 1 in Figure 5 is observed at a binding energy of 405.0 eV relative to the vacuum level. This peak gains intensity with increasing NH_3 exposure. In addition to this main peak, a small peak, labeled 2, is observed at 403.0 eV and contributes to the broad and asymmetric appearance of the main NH_3 nitrogen 1s peak, especially at low coverages. On the basis of the literature[3,4,15,16,19,57] XPS nitrogen 1s data for molecularly adsorbed NH_3 species, peak 2 can be assigned to chemisorbed NH_3, and the strong peak at 405.0 eV to physisorbed NH_3. These assignments are consistent with the valence band studies in section III.A1, which show the coexistence of chemisorbed and physisorbed molecular NH_3 on the ZnO surface, particularly at higher NH_3 coverages. Physisorbed NH_3 remains on the surface during the period of data accumulation even at UHV because the sample temperature is maintained at 130 K, much lower than the NH_3 melting point[49] (195 K). Also observed in Figure 5 is an additional weak peak (3) at 400.4 eV. It appears at low NH_3 exposures and remains even at high coverages. On the basis of the nitrogen 1s core energies reported for surface nitrides,[4,15,16,24] the observation of peak 3 may indicate the presence of a limited amount of deprotonated NH_3 on ZnO-(0001) at low temperatures.

The effective atomic charge, Q, on the nitrogen atom of chemisorbed NH_3 can be estimated using the charge potential model:[58,59]

$$\Delta E_{PES} = kQ + V + L \qquad (5)$$

Here ΔE_{PES} is the shift in the core-level ionization potential of the ammonia nitrogen atom with respect to that of a standard compound (N_2 at 409.9 eV,[58] which serves as the origin for the energy scale). The total binding energy shift for a nonbonding level on chemisorption, ΔBE_{PES}, results from an extramolecular relaxation polarization shift, ΔR (a final state effect, in which the core hole on the adsorbate molecule created by photoemission is partly screened through polarization of electrons from the substrate, resulting in a peak shift to lower binding energy), and from effects of the change in chemical environment, ΔE_{PES} (an initial state effect caused by redistribution of valence electron density between an adsorbate molecule and the substrate due to bonding, shifting the peak to deeper binding energy as the net positive charge on the atom increases):

$$\Delta BE_{PES} = \Delta E_{PES} - \Delta R \qquad (6)$$

The effective atomic charge of the adsorbed NH_3 is closely related to ΔE_{PES}, rather than the total energy shift ΔBE_{PES}. The core relaxation, ΔR_c, can be obtained from the energy shift of a corresponding Auger line. Here we use $\Delta R = 2.0$ eV obtained from CO/ZnO.[31] Thus, for chemisorbed NH_3 (peak 2 in Figure 5) $\Delta BE_{PES} = -6.9$ eV and $\Delta E_{PES} = -4.9$ eV relative to N_2. V in eq 5 is the Coulomb potential energy at the nitrogen position generated by the other atoms in the lattice ($V = \sum(Q'/r)$, in which Q' is the charge on the non-nitrogen atoms estimated from the half-ionized core model, r is the distance from each atom to the nitrogen atom, and the sum is over all atoms).[60] k and L are Jolly's empirical parameters determined from a least-squares fit for a large series of chemical shifts of an element (for nitrogen, $k = 25.06$ and $L = 0.57$).

The effective atomic charge on the nitrogen atom of NH_3/ZnO(0001) is calculated from eq 5 to be $Q = -0.34$ unit charge.

(54) A 1.4 ± 0.1 eV decrease in the work function, due to the change in the surface dipole moment, is found for the ZnO(0001) surface.
(55) Thomas, J. M.; Thomas, W. J. *Introduction to The Principles of Heterogeneous Catalysis*; Academic Press: London, 1967; p 134.
(56) On the basis of a dipole–dipole repulsion calculation, the lowest energy NH_3-saturated ZnO(11$\bar{2}$0) surface would be the p(2 × 1) overlayer, which gives a $\theta_{sat} = 0.5$ (see: Cohen, S. Ph.D. Dissertation, MIT, Boston, MA, 1985).
(57) Cochran, S. J.; Larkins, F. P. *J. Chem. Soc., Faraday Trans. 1* **1986**, *82*, 1721.
(58) Siegbahn, K.; Nordling, C.; Johansson, G.; Hedman, J.; Heden, P. F.; Hamrin, K.; Gelius, U.; Bergmark, T.; Werme, L. O.; Manne, R.; Baer, Y. *ESCA Applied to Free Molecules*; North-Holland Publishing Co.: Amsterdam, 1969.
(59) Jolly, W. L. *Faraday Disc. Chem. Soc.* **1972**, *54*, 13.
(60) Using $Q_H' = 0.6$, $Q_O' = -1.9$, $Q_{Zn}' = 1.7$, $r_{Zn-N} = 2.04$ Å, $r_{O-N} = 3.56$ Å, and $r_{H-N} = 1.01$ Å, we obtain $V = \sum Q'/r = 3.0$ for the nitrogen site in the $[ZnO_3NH_3]^{4-}$ cluster. Note that all Q's estimated from the half-ionized core model should be multiplied by 0.2 when used to obtain V.[59]

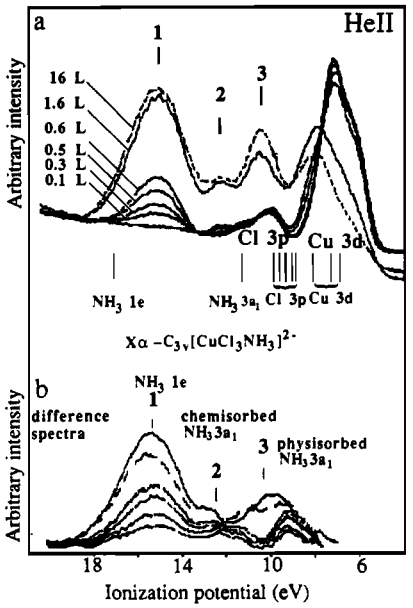

Figure 6. He II valence band spectra of NH_3 on CuCl(111). Part a shows data for the CuCl(111) surface exposed to the NH_3 langmuirs (L) listed. At low ammonia exposures the spectra have been aligned to the Zn 3d band and at higher coverages (> 0.5 L) to the NH_3 band. Part b gives the NH_3-covered minus clean CuCl(111) difference spectra at a variety of NH_3 coverages. The calculated SCF-Xα-SW ionization energies for $[CuCl_3NH_3]^{2-}$ are included below the experimental UPS data for comparison.

The charge on the nitrogen atom of gas phase NH_3 calculated using the same procedure is −0.40. The net decrease in the negative charge on the nitrogen of $\Delta Q = 0.06$ corresponds to the electron density transferred from adsorbed NH_3 to ZnO and is close to the results obtained from work function measurements in section III.A2.

B. PES Study of NH_3/CuCl(111). 1. Valence Band Photoemission and Heat of Adsorption. Figure 6a shows the He II valence band spectrum for clean CuCl(111) and the surface exposed to various NH_3 doses at 140 K. The clean CuCl spectrum consists of two major peaks arising from chlorine 3p and copper 3d orbitals at energies centered at approximately 11 and 7 eV below the vacuum level. Upon exposure to NH_3 (0.1–0.6 L), two new peaks (labeled 1 and 2 in Figure 6a) appear at 15.5 and 12.5 eV. Increasing the NH_3 exposure leads to the observation of a new peak, 3, as well as the further increase in the intensity of peaks 1 and 2. At high coverages (>1.6-L exposure), the Cu 3d band is greatly attenuated, and peaks 1 and 3 become particularly evident. Peak 3 is superimposed over the chlorine 3p band and is centered at ~10.1 eV. The energy separation between peaks 1 and 3 is 5.4 eV, which is equal to the $3a_1$–1e splitting in gaseous NH_3 (see Figure 2). On the basis of this splitting, bands 1 and 3 are assigned as arising from physisorbed NH_3, with peak 1 the ammonia 1e level and peak 3 the $3a_1$ level. Peaks 1 and 2 appear to gain intensity at the same rate at low NH_3 coverages, thus they most likely correspond to the same species, i.e. chemisorbed NH_3. Note that peak 1 is broad and is a composite peak of the overlapping physisorbed and chemisorbed 1e levels. Peak 2 is assigned as the $3a_1$ orbital for chemisorbed NH_3 (vide infra, section III.c). The $3a_1$–1e splitting for NH_3 on CuCl(111) is ~3 eV, which gives a $3a_1$ stabilization of 2.4 eV upon binding to the surface. The 2.4 eV stabilization of the $3a_1$ in the NH_3/CuCl system is significantly larger than the 1.4 eV stabilization observed for the NH_3/ZnO(0001) surface (section III.A1).

Increasing sample temperature results in the decrease in the intensity of the NH_3 1e peak, indicating that molecular NH_3 desorbs. The intensity of the NH_3 1e peak, which reflects the surface coverage, depends on the sample temperature and the ambient NH_3 pressure at equilibrium. Thus, this peak is used to determine the heat of adsorption of NH_3 on CuCl(111). Fixed ambient NH_3 pressures were maintained, and He II UPS spectra

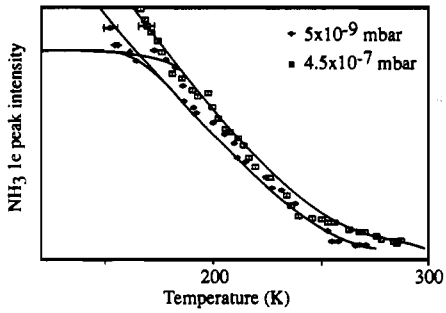

Figure 7. Variation in the equilibrium coverage of NH_3 on the CuCl(111) surface as a function of temperature for 5×10^{-9} mbar and 4.5×10^{-7} mbar NH_3 ambient pressures. Data have been fit to two Temkin isobars: one for chemisorption yielding $\Delta H_0 = 24 \pm 3$ kcal/mol and the other for physisorption with $\Delta H = 6 \pm 3$ kcal/mol.

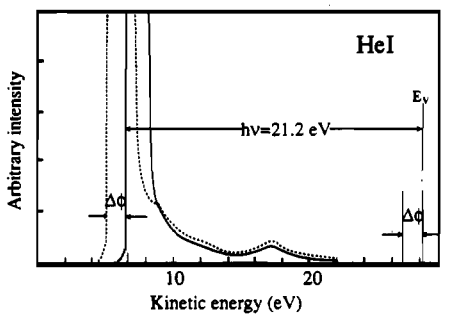

Figure 8. He I UPS study of the work function change of the CuCl(111) surface upon NH_3 adsorption. The solid line is the He I UPS spectrum for the clean CuCl(111) surface, while the dashed line is for the CuCl(111) surface exposed to 3 L of NH_3 at 140 K. The spectra are aligned to the Cl 3p band to correct for changes in band bending. The 1.3-eV shift to lower kinetic energy in the onset of the secondary electron tail corresponds to the surface dipole moment change upon NH_3 adsorption.

were collected at a series of temperatures. Figure 7 presents the NH_3 1e peak area versus temperature for two ambient NH_3 pressures (5×10^{-9} and 4.5×10^{-7} mbar). As found in the NH_3/ZnO(0001) system, there is a linear decrease of $\Delta H(\theta)$ with increasing coverage, θ. Following the same procedure as presented in section III.A1, the heat of adsorption extrapolated to zero coverage is found to be 24 ± 3 kcal/mol for the NH_3/CuCl(111)[64] and 6 ± 3 kcal/mol for the physisorbed layer, which are very similar to the 28 ± 3 and 6 ± 3 kcal/mol observed for NH_3/ZnO(0001). (The data corresponding to intermediate coverages in Figure 7 are not well separated for the CuCl surface due to problems achieving equilibrium under the experimental conditions required to collect the spectrum. The ΔH_0 value quoted was thus estimated from a Clausius–Clapeyron analysis of the low-coverage data.)

2. NH_3–CuCl(111) Dipole Moment. CuCl is an extrinsic p-type semiconductor,[52] where the presence of some Cu(II) ions results in acceptor levels located just above the top of the valence band. In contrast to ZnO, CuCl possesses a downward band bending[53] and the change in its surface work function upon NH_3 chemisorption is given by

$$\Delta\Phi = \Delta\Phi_{dipole} - \Delta\Phi_{bb} \qquad (7)$$

where $\Delta\Phi_{dipole}$ is the change in the surface dipole moment and $\Delta\Phi_{bb}$ is the contribution from surface band bending. In Figure 8 changes due to band bending are corrected by aligning the Cl 3p band of the NH_3-covered surface with that of the clean surface. The energy shift in the threshold of the secondary electron tail then gives a decrease in the surface dipole moment by 1.3 ± 0.2 eV, due to NH_3 adsorption (3 L of NH_3 at 140 K). Using the Helmholtz equation presented in section III.A2 with $\theta = 1$ and $\beta = 0$ for the chemisorbed NH_3-saturated CuCl(111) surface, this dipole moment change gives a value for the apparent dipole moment of $\mu = 0.5$ D negative side down. Combined with the 2.4-eV bonding stabilization of the NH_3 $3a_1$ orbital observed in section III.B1, the decrease in the surface dipole moment confirms

Table II. Ground-State Energies (eV), Slater Transition-State Energies (eV), and Valence Charge Decomposition (%) for $[ZnO_3NH_3]^{4-}$ [a]

level	ground state	transition state	Zn(s)	Zn(p)	Zn(d)	Zn(f)	O(s)	O(p)	O(d)	N(s)	N(p)	N(d)	H(s)
7e	−3.3425	−5.8487		5.34	11.96	0.92	0.20	81.34	0.15		0.00	0.06	0.03
$1a_2$	−3.6286	−6.1217				1.23		98.73	0.04				
6e	−3.8309	−6.2957		0.49	4.94	0.58	0.00	93.81	0.06		0.08	0.01	0.03
$6a_1$	−3.9943	−6.4476	2.18	0.04	12.25	0.87	0.00	77.76	0.03	0.96	5.55	0.03	0.32
5e	−4.4823	−6.9277		10.05	2.17	0.14	0.11	86.91	0.08		0.07	0.25	0.21
$5a_1$	−5.2636	−7.7801	12.15	7.51	5.03	0.36	0.67	68.22	0.32	0.40	5.09	0.01	0.25
$4a_1$	−7.0607	−10.9764	9.51	1.08	55.23	0.40	0.87	19.24	0.62	0.45	11.82	0.00	0.78
4e	−7.5127	−13.8165		0.05	94.05	0.00	0.04	4.66	0.43		0.16	0.28	0.31
3e	−7.6990	−13.8780		0.11	87.48	0.03	0.57	11.13	0.60		0.00	0.05	0.04
$3a_1$	−9.2692	−13.6382	4.82	3.11	29.45	0.51	0.07	0.11	0.01	1.64	54.81	0.87	4.59
2e	−14.0254	−19.9103		0.05	0.27	0.04	0.02	0.00	0.00		58.58	5.54	35.48
1e	−18.1089	−20.7259		2.06	1.92	0.22	95.72	0.05	0.02		0.01	0.00	0.00
$2a_1$	−18.3037	−20.9124	3.72	0.51	0.47	0.68	94.35	0.16	0.03	0.02	0.03	0.00	0.12
$1a_1$	−23.2572	−29.1246	0.26	0.31	0.25	0.07	0.01	0.00	0.00	72.18	1.86	0.63	24.42

[a] The charge decomposition is atom degeneracy weighted so that all levels sum to 100%.

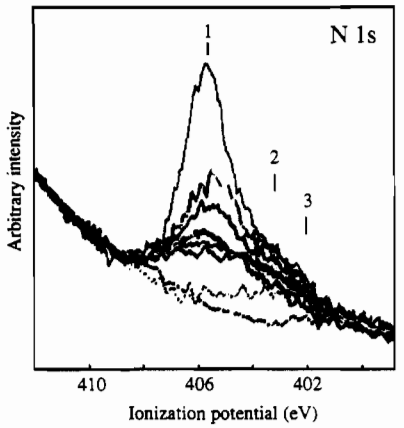

Figure 9. XPS nitrogen 1s spectra of the NH_3-covered CuCl(111) surface at 140 K. From bottom to top, the NH_3 dose increases in the order 0.01, 0.1, 0.3, 0.5, 0.6, 1.6, and 16 L followed by long exposure to a 4 × 10^{-8} mbar NH_3 ambient. Energies for peaks 1–3 were determined by Gaussian/Lorentzian fits of the experimental data.

that NH_3 is bound to the surface via its nitrogen atom and that the NH_3 molecule transfers electron density from the nitrogen lone pair to the surface. The calculation of charge transfer based on the above results is complicated by possible contributions from the intrinsic dipole moment of NH_3 (1.47 D for gas phase, which is larger than the 0.5 D caused by adsorption) and the adsorption-induced change in the substrate surface dipole moment. More direct information on the charge transfer is obtained from the N 1s core level study described below.

3. Nitrogen 1s Core Level and Effective Atomic Charge. Figure 9 gives the XPS nitrogen 1s core spectra for various NH_3 exposures on CuCl(111) at 140 K. At low exposures (0.1 L) a broad peak is observed centered at 403.5 eV (peak 2) relative to the vacuum level. On the basis of the parallel UPS study in section III.B1, molecular chemisorption dominates at this stage. Peak 2 is assigned as chemisorbed NH_3. Increasing the NH_3 coverage results in a new peak, labeled 1, centered at 405.8 eV below the vacuum level. This peak increases in intensity with increasing NH_3 exposures and can be assigned to physisorbed NH_3, since it is dominant at high coverages and low temperatures (below 190 K). Compared with chemisorbed NH_3, physisorbed NH_3 is bound to the substrate more weakly and thus shows a smaller extramolecular relaxation polarization shift, which is responsible for the large shift (approximately 2 eV) of the nitrogen 1s peak to deeper binding energy relative to peak 2. Peak 2, corresponding to chemisorbed NH_3, gains intensity with increasing NH_3 dose until the sample is in equilibrium with a 1 × 10^{-7} mbar NH_3 ambient. Peak 2 does not grow as rapidly as peak 1, in agreement with the previous observation that NH_3 clustering occurs before a monolayer is completed.

As the NH_3-covered surface is slowly warmed to 190 K, the intensity of peak 1 decreases significantly. (Note that this temperature is close to the NH_3 melting point, 195 K.) If the temperature is further increased to ~300 K, the intensity of peak 2 is reduced and a broad peak remains centered at about 402 eV below the vacuum level (peak 3 in Figure 9). Peak 3 is assigned to surface nitride resulting from a limited amount of NH_3 deprotonation on CuCl(111). Its energy position is close to the values reported for surface nitride in the literature.[4,15,16,24] Peak 3 is also observed at very low coverages (0.01 L) at low temperatures.

It is possible to estimate the effective atomic charge, Q, on the nitrogen atom of chemisorbed NH_3 according to the charge potential model (see section III.A3). The effective atomic charge on the nitrogen atom of NH_3/CuCl(111) calculated using ΔE_{PES} = −3.5 eV (relative to N_2 for the relaxation corrected chemisorbed NH_3, based on ΔBE_{PES} = −6.4 eV and ΔR = 2.9 eV obtained[31] from CO/CuCl)[61] is Q = −0.31 unit charge. Compared to the effective atomic charge on the nitrogen atom of gas phase NH_3 (−0.40), the net decrease of charge on the nitrogen atom is ΔQ = 0.09. This corresponds to electron density transferred from adsorbed NH_3 to the CuCl surface, which is larger than the 0.06 obtained for NH_3/ZnO(0001), indicating stronger covalent bonding of NH_3 to Cu(I). This is consistent with the smaller $3a_1$–1e splitting observed for NH_3 on CuCl relative to ZnO and indicates a greater stabilization of the nitrogen lone pair by Cu(I) although the heat of adsorption data are found to be similar for both surface sites (24 ± 3 and 28 ± 3 kcal/mol for Cu(I) and Zn(II), respectively). These results can be analyzed in detail through the Xα calculations as presented below.

C. SCF–Xα–SW Calculations on $[ZnO_3NH_3]^{4-}$ and $[CuCl_3NH_3]^{2-}$. Tables II and III summarize the ground-state energies, Slater transition-state ionization energies, and valence level atomic charge decompositions for $[ZnO_3NH_3]^{4-}$ and $[CuCl_3NH_3]^{2-}$ obtained using the parameters listed in Table I. Figures 1 and 6 show the calculated ionization energies juxtaposed with the experimental UV photoelectron spectra. As can be seen in the figures, the qualitative energy order and peak position for the calculated UP spectrum are in reasonable agreement with the experimental data.

For $[ZnO_3NH_3]^{4-}$ (Figure 1), Xα places the oxygen 2p orbitals at highest energy with binding energies ranging from 5.8 to 11.0 eV (levels 7e–$5a_1$ in Table II). Experimentally, this band is found at binding energies ranging from 7 to 13 eV. The zinc d orbitals are calculated to have binding energies between 11.0 and 13.8 eV (Table II, levels $4a_1$–3e). This is slightly below the observed zinc 3d band which is centered at ~15.0 eV relative to the vacuum level. Level $4a_1$ at ~11.0 eV is somewhat shifted from the remaining 3d orbitals. Level $4a_1$ has ~55% Zn d_{z^2} character and ~30% N p_z character in the transition state, and the increased nitrogen character destabilizes this orbital relative to the other d orbitals. The calculations place the ammonia $3a_1$ orbital at a

(61) Using Q_H = 0.6, Q_{Cl}' = −0.8, Q_{Cu}' = 0.4, r_{Cl-N} = 3.39 Å, r_{Cu-N} = 2.07 Å, and r_{H-N} = 1.01 Å, we obtain $V = \sum Q'/r$ = 3.8 for the nitrogen site in the $[CuCl_3NH_3]^{2-}$ cluster. Note that all Q's should be multiplied by 0.2 to obtain V.[59]

Table III. Ground-State Energies (eV), Slater Transition-State Energies (eV), and Valence Charge Decomposition (%) for $[CuCl_3NH_3]^{2-}$[a]

level	ground state	transition state	Cu(s)	Cu(p)	Cu(d)	Cu(f)	Cl(s)	Cl(p)	Cl(d)	N(s)	N(p)	N(d)	H(s)
$6a_1$	−2.7878	−6.6644	0.76	5.24	72.77	0.31	0.13	7.32	1.70	0.69	10.38	0.10	0.60
7e	−3.1362	−7.0506		2.24	82.37	0.11	0.22	12.17	2.01		0.11	0.41	0.36
6e	−3.5000	−7.8356		0.03	93.49	0.00	0.00	4.57	0.92		0.18	0.40	0.41
$1a_2$	−5.9161	−8.5714				0.54		99.43	0.02				
5e	−6.1056	−8.7378		0.09	3.10	0.41	0.00	95.65	0.03		0.32	0.11	0.28
$5a_1$	−6.3542	−8.9990	0.32	2.33	24.12	0.54	0.00	37.37	0.07	1.02	30.89	0.56	2.78
4e	−6.4174	−9.0401		0.15	10.81	0.19	0.00	88.60	0.18		0.05	0.00	0.02
$4a_1$	−6.4779	−9.5136	0.52	7.88	2.99	0.12	0.01	61.46	0.06	0.37	23.76	0.37	2.45
3e	−6.6210	−9.2886		6.50	9.70	0.19	0.11	83.18	0.24		0.04	0.00	0.03
$3a_1$	−7.4491	−10.8709	22.62	0.00	0.01	0.94	0.81	61.97	0.46	0.06	11.55	0.24	1.34
2e	−10.4184	−16.3898		0.14	0.45	0.07	0.02	0.10	0.00		60.94	4.35	33.93
1e	−17.8069	−20.6270		1.21	0.89	0.12	97.75	0.02	0.00		0.00	0.00	0.00
$2a_1$	−17.9279	−20.7353	2.08	0.34	0.25	0.36	96.63	0.08	0.02	0.14	0.02	0.00	0.07
$1a_1$	−19.7917	−25.8379	0.44	0.47	0.36	0.11	0.09	0.00	0.00	74.22	1.38	0.43	22.49

[a] The charge decomposition is atom degeneracy weighted so that all levels sum to 100%.

binding energy of 13.6 eV (Table II, level $3a_1$). This agrees with the experimentally observed band which grows with low ammonia coverage (i.e. due to chemisorbed ammonia) at ~13.2 eV, as is evident in the difference spectrum shown in Figure 1. The breakdown of the atomic charges in the Slater transition state for this level unambiguously identify it as the ammonia $3a_1$ level [the major components are 66.88% N(p_z), 5.00% H(s), 4.29% Zn(4s), 3.52% Zn($4p_z$), and 16.31% Zn(d_{z^2})]. The deepest binding energy band shown in Figure 1 is assigned as the ammonia 1e level (level 2e in Table II). The wave function obtained for the transition state of this level is composed of 57.08% N($p_{x,y}$) and 35.48% H(s). The binding energy predicted by Xα for this band, 19.91 eV, is deeper than the observed value of ~18 eV. The calculated ammonia $3a_1$–1e splitting for the ZnO surface is 6.27 eV, which is only marginally reduced by 0.25 eV from that calculated for gaseous ammonia (6.53 eV, experimental result = 5.4 eV).

For $[CuCl_3NH_3]^{2-}$, as shown in Figure 6, Xα calculates that the highest lying band at 6–8 eV binding energy is the copper d manifold. Xα assigns low binding energy shoulder of this band as the d_{z^2} (Table III, level $6a_1$) orbital (which interacts most strongly with the nitrogen lone pair of electrons) and the remaining 3d orbitals are split over two doubly degenerate levels (7e and 6e in Table III). Xα places the chlorine 3p band to deeper binding energy at 9–12 eV (levels $1a_2$–3e in Table III), which is consistent with the experimental data. At a binding energy of ~10.9 eV is a band that Xα assigns as the ammonia $3a_1$ orbital. Examination of Table III shows that three levels ($5a_1$, $4a_1$, $3a_1$) all have appreciable nitrogen p_z character. This indicates that the nitrogen lone pair is covalently mixed over these levels in the ground state and would imply that no single level can be assigned to the ammonia $3a_1$ level. Upon ionization, however, the Xα calculated charge density becomes strongly localized with only one orbital (corresponding to level $3a_1$ in Table III) having appreciable nitrogen p_z character [the charge distribution in the transition state is 60.21% N(p_z), 5.11% H(s), 12.87% Cu(4s), 3.44% Cu(4p), 7.52% Cu($3d_{z^2}$), and 7.22% Cl(p)]. This allows the ~12-eV binding energy band in the UPS spectrum (labeled 2 in Figure 6) to be assigned to the $3a_1$ state of chemisorbed ammonia. Xα predicts this band to occur at 10.9 eV, which is in reasonable agreement with experimental value. Finally, the ~15.5-eV band (labeled 1 in Figure 6) is assigned as the ammonia 1e level (level 2e in Table II). The charge decomposition in the transition state for this level is 60.17% N($p_{x,y}$) and 34.38% H(s). The splitting of the $3a_1$–1e levels is calculated to be 5.52 eV, which is reduced by approximately 1 eV over that calculated for gaseous ammonia. Details on ammonia bonding will be expanded upon in the following section.

IV. Discussion

The UPS studies have shown that a shift in the NH_3 $3a_1$ level (ΔE_{3a_1} in Table IV) occurs upon ammonia chemisorption to both ZnO and CuCl surfaces, with ΔE_{3a_1} = 1.4 eV for NH_3/ZnO(0001) and 2.4 eV for NH_3/CuCl(111). Nitrogen 1s core level studies find that charge is transferred from the adsorbed NH_3 to the ZnO and CuCl surfaces; $(\Delta q)_{XPS}$ = ~0.06 for NH_3/ZnO(0001) and 0.09 for NH_3/CuCl(111), which is in agreement with the observation of a decrease in the surface dipole moment ($\Delta\Phi$) upon NH_3 adsorption (by −1.4 eV on ZnO(0001) and by −1.3 eV on CuCl(111)). With these observations, and the results of the electronic structure calculations, it is possible to obtain a description of σ bonding in these d^{10} metal ion surface complexes.

Table IV. Comparison of NH_3 Binding to Zn(II) and Cu(I) Sites

	Zn(II)	Cu(I)		Zn(II)	Cu(I)
$\Delta E(3a_1)$, eV	1.4	2.4	ΔH_0, kcal/mol	28	24
nitrogen Δq (XPS)	0.06	0.09	W_{el}, kcal/mol	17	9
surface $\Delta\Phi_{dipole}$, eV	−2.1	−1.3	W_{co}, kcal/mol	11	15

Table V. SCF–Xα–SW Description of Ammonia Bonding In $[CuCl_3NH_3]^{2-}$ and $[ZnO_3NH_3]^{3-}$[a]

compd	Δ(% 4s)	Δ(% 4p)	% 3d[b]	$3a_1$ − 1e[c]
$[CuCl_3NH_3]^{2-}$	3.20	13.25	7.52	5.519
$[ZnO_3NH_3]^{4-}$	−0.87	5.20	16.31	6.139

[a] Metal 4s and 4p contributions to NH_3 bonding were determined as follows: SCF–Xα–SW calculations were performed on $[CuCl_3]^{2-}$ and $[ZnO_3]^{4-}$ (using the same parameters as in the NH_3 complexes; see supplementary material) and the metal 4s and 4p bonding interactions were tabulated. These values were then subtracted from the results obtained from the full calculation—the difference giving the change in metal bonding upon ammonia coordination. [b] % d_{z^2} character in the Slater transition state of the $3a_1$ orbital in ammonia. [c] Splitting of the nitrogen lone pair ($3a_1$) and N–H bond (1e) in eV; the Xα-calculated splitting for gas-phase ammonia is 6.527 eV (experimental result = 5.4 eV).

Bonding between NH_3 and the surface metal ion sites can be factored into two contributions: electrostatic and covalent. The electrostatic interaction arises from the attraction of the dipole of the NH_3 molecule to the positively charged metal ion. Covalent bonding results from the participation of the unoccupied metal 4s and 4p orbitals and their ability to accept electron density from the lone pair of σ electrons on the nitrogen atom. Note, the metal d orbitals can interact with the ammonia molecule (shifting the NH_3 $3a_1$ orbital energy), but because the d orbitals are filled in these d^{10} systems, this interaction cannot contribute to net bonding. Using the experimental heat of adsorption measurements presented earlier, and the integrated charge of the metal ion sites from the SCF–Xα–SW calculations, it is possible to estimate the relative contributions of each bonding interaction for both surfaces.

Heat of adsorption measurements show that NH_3 has a slightly stronger interaction with the ZnO(0001) surface (ΔH_0 = 28 ± 3 kcal/mol) than with the CuCl(111) surface (24 ■ 3 kcal/mol). The electrostatic contribution can be calculated using a point dipole approximation. The energy of the electrostatic interaction, W_{el} (el = electrostatic), between a dipole moment, μ, and an ion with charge Z is given by[62]

$$W_{el} = Z\mu/4\pi r^2\epsilon_0 \qquad (8)$$

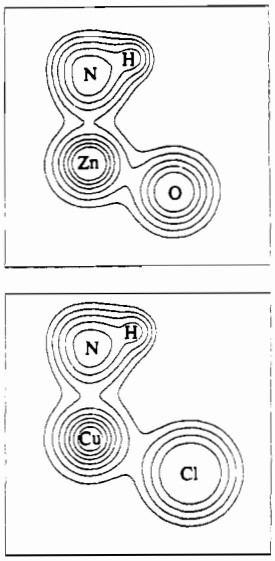

Figure 10. Total electron density contour plots for $[ZnO_3NH_3]^{4-}$ (top) and $[CuCl_3NH_3]^{2-}$ (bottom). The *xz* plane is shown (i.e. contains the 3-fold rotation axis, the metal nitrogen bond, and an in-plane metal oxide (chloride) and N–H bond). Contour levels are 0.04, 0.08, 0.16, 0.32, 0.64, 1.28, and 2.56 e/bohr^3. Core-level electron density has been omitted for clarity.

where r is the distance between the ion and the midpoint of the molecular dipole and ϵ_0 is the permittivity of a vacuum ($\epsilon_0 = 2.66 \times 10^{14}$ D/eV cm^2). For $[ZnO_3NH_3]^{4-}$ and $[CuCl_3NH_3]^{2-}$, integration of the scattered wave solutions[36] within the sphere boundaries of the metal ion gives zinc a +1.07 charge and the Cu ion +0.56. Using the above formula with $r \cong 2.3$ Å (the distance between the Zn(II) and Cu(I) ions to the midpoint of the ammonia dipole) and $\mu(NH_3) = 1.47$ D (the gas-phase value), the estimated electrostatic interaction energy for NH_3/ZnO(0001) is 17 kcal/mol. For the Cu(I) ion, with only $\sim^1/_2$ the charge as the Zn(II) ion, the electrostatic interaction energy is ~9 kcal/mol. Subtracting the calculated electrostatic bond energy from the measured heat of adsorption gives a covalent interaction (W_{cov}) of ~11 kcal/mol for NH_3/ZnO(0001) and ~15 kcal/mol for NH_3/CuCl(111). On the basis of this simplified ion–dipole model, the covalent contribution to bonding is stronger for NH_3/CuCl(111) than for NH_3/ZnO(0001). These results agree with our prior results for the adsorption of CO on CuCl and ZnO.[31]

The SCF–Xα–SW results can be used to obtain further insight into the covalent contribution to bonding. Table V gives the change in the metal 4s and 4p bonding contributions which occur upon ammonia coordination. These values were obtained by subtracting the percent 4s and 4p character obtained for the clean surface models ($[ZnO_3]^{4-}$ and $[CuCl_3]^{2-}$ using identical sphere radii, outer and Watson spheres, geometry, etc.; see supplementary material) from the full calculations including the NH_3 group. Consistent with the above experimental results, the calculated bonding changes show that Cu(I) interacts much more covalently with NH_3 than does Zn(II). Upon NH_3 binding, the $[CuCl_3NH_3]^{2-}$ model gains 3% 4s and 13% 4p character, while the Zn(II) site in $[ZnO_3NH_3]^{4-}$ is calculated to lose ~1% 4s and gain only 5% 4p character. Total electron density contours for $[ZnO_3NH_3]^{4-}$ and $[CuCl_3NH_3]^{2-}$ are presented in Figure 10. The greater degree of covalency in the Cu(I) model is evident by the increased total electron density between the nitrogen atom and the Cu(I) ion relative to the rather narrow contour bridge connecting the ammonia to the Zn(II) site.

The interaction between the NH_3 $3a_1$ and the unoccupied metal ion $4p_z$ orbital appears to dominate the covalent contribution to σ bonding. In principle this should decrease the $3a_1$–1e splitting, and in fact a smaller splitting is observed and calculated for Cu(I)

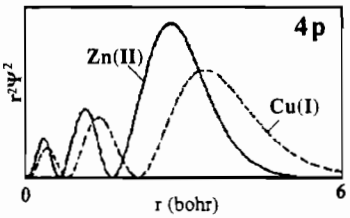

Figure 11. Plot of the 4p radial probability function for Cu(I) ($Z_{eff} = 3.7$) and Zn(II) ($Z_{eff} = 4.7$). Z_{eff} (effective atomic charge) values were calculated using Slater's Rules.[62]

than for the Zn(II) site. However this is complicated by the additional covalent interaction of the d band, which is filled and thus does not contribute to net bonding. Interaction between two levels A and B should produce an energy stabilization of the $3a_1$ orbital, ΔW, which is approximately[63]

$$\Delta W \cong -(H_{AB})^2/\Delta E \qquad (9)$$

where the resonance integral $H_{AB} = \langle A|H|B\rangle$ and ΔE is the energy difference between these orbitals. For the $3a_1$–3d interaction, ΔE is positive for Cu(I) and negative for Zn(II). The Xα charge decomposition given in Table V shows that the d band does interact with the $3a_1$ orbital (7.5% for CuCl and 16.3% for ZnO). Thus, the $3a_1$–1e splitting is not a direct parameter to describe the difference in bonding interactions. Equation 9 further provides insight into the electronic origin of the increased 4p covalent bonding interaction with the Cu(I) site. The energies of the 4p orbital for Cu(I) and Zn(II) are very similar (2.2 eV for Zn(II) and 2.8 eV above the vacuum level for Cu(I)[64]); thus, the ΔE values in eq 9 are nearly the same for both surfaces. The observed stronger covalent σ bonding for NH_3/Cu(I) must then result from differences in H_{AB}, with H_{AB} being larger for Cu(I) than for Zn(II), thus its increased covalency. H_{AB} in the Wolfsberg–Helmholtz approximation is proportional to the overlap between the NH_3 $3a_1$ and the metal 4p orbitals. The additional nuclear charge on Zn(II) causes its electron cloud to contract more tightly about the nucleus and is therefore less available for overlap. A plot of the 4p radial distribution function for Zn(II) and Cu(I) exhibiting this radial contraction is shown in Figure 11.

In summary, the heats of adsorption for NH_3 bonding to Zn(II) versus Cu(I) surface sites show the interaction is slightly stronger for the Zn(II) site. The ionic contribution to this interaction is larger for the Zn(II) site, and using the charge distribution obtained from the Xα calculation its magnitude is estimated to be 17 kcal/mol. The electrostatic interaction between the Cu(I) ion and the ammonia dipole was calculated to be only 9 kcal/mol. The resultant σ-bond contributions to the heat of adsorption are 11 and 15 kcal/mol for ZnO and CuCl, respectively. The ammonia $3a_1$ σ-bonding interaction is thus found to be greater for Cu(I) than for Zn(II) sites, and this conclusion is supported by Xα calculations. The increased covalency in the Cu(I) system was found to result from an increase in the resonance integral H_{AB} for Cu(I) which arises from the increased radial expansion of the Cu(I) 4s and 4p orbitals relative to the more contracted Zn(II) orbitals. The NH_3 $3a_1$–1e energy splitting was found to not be a reliable indicator of the degree of covalency in these systems, as an appreciable amount of metal d character is mixed into the $3a_1$ orbital and perturbs its energy in opposite directions for Zn(II) and Cu(I) sites.

Acknowledgment. We thank Professor J. C. Merle of Universite Louis Pasteur for providing the CuCl single crystal used in this study and Professor Victor Henrich for use of his instrumentation during the early phase of this work. This work is supported by the NSF-MRL Program through the Center for Materials Re-

(62) Huheey, J. E. *Inorganic Chemistry*, 2nd ed.; Harper and Row: New York, 1983; p 238.

(63) Pauling, L.; Wilson, E. B., Jr. *Introduction to Quantum Mechanics With Applications to Chemistry*, 2nd ed.; Dover Publications: New York, 1963; p 195.

(64) Atomic Energy Levels. *Nat. Bur. Stand. Circ. (U.S.)* **1952**, *No. 467*.

search at Stanford University. Support for the work done at Stanford Synchrotron Radiation Laboratory, which is operated by the Department of Energy, Division of Chemical Sciences, is gratefully acknowledged. P.M.J. would also like to acknowledge the IBM Corp. for its financial support.

Registry No. ZnO, 1314-13-2; CuCl, 7758-89-6; NH_3, 7664-41-7.

Supplementary Material Available: Tables giving the ground-state energies and valence level charge decomposition (%) for $[ZnO_3]^{4-}$ and $[CuCl_3]^{2-}$ (2 pages). Ordering information is given on any current masthead page.

Contribution from the Département de chimie, Université de Sherbrooke, Sherbrooke, Québec, Canada J1K 2R1, and Contribution No. 8446 from the Arthur Amos Noyes Laboratory, California Institute of Technology, Pasadena, California 91125

Silver and Gold Dimers. Crystal and Molecular Structures of $Ag_2(dmpm)_2Br_2$ and $[Au_2(dmpm)_2](PF_6)_2$ and Relation between Metal-Metal Force Constants and Metal-Metal Separations

Daniel Perreault,[1a] Marc Drouin,[1a] André Michel,*[,1a,c] Vincent M. Miskowski,[1b] William P. Schaefer,*[,1b,c] and Pierre D. Harvey*[,1a]

Received June 21, 1991

The $Ag_2(dmpm)_2Br_2$ and $[Au_2(dmpm)_2](PF_6)_2$ compounds (dmpm = bis(dimethylphosphino)methane) have been characterized by X-ray diffraction at 298 K. The molecules are found to contain $M_2(dmpm)_2^{2+}$ core structures with two metal atoms bridged by the dmpm ligands to give eight-membered $M_2P_4C_2$ rings. The silver compound forms a polymeric chain where the silver atoms of adjacent $Ag_2(dmpm)_2^{2+}$ units are linked by two Br anions (r(AgBr) = 2.7431 (13), 2.9453 (14) Å). The intra- and intermolecular Ag···Ag separations are 3.605 (2) and 3.916 (2) Å, respectively, while the Au···Au distance in $[Au_2(dmpm)_2](PF_6)_2$ is 3.045 (1) Å. In the latter case, some weak Au···F contacts (r(AuF) = 3.44 (1) Å) are also noticed. The solid-state low-frequency (40-400 cm^{-1}) vibrational spectra of these compounds and five other related complexes containing Ag_2 and Au_2 have been analyzed. Intense Raman scatterings associated with the metal-metal stretching frequencies ($\nu(M_2)$) along with the metal-metal force contants ($F(M_2)$; estimated from the diatomic approximation) have been obtained. The $\nu(M_2)$ (cm^{-1}) and $F(M_2)$ (mdyn $Å^{-1}$) values are as follows, respectively: $[Ag_2(dmpm)_2](PF_6)_2$, 76 and 0.18; $[Ag_2(dppm)_3](PF_6)_2$ (dppm = bis(diphenylphosphino)methane), 76 and 0.18; $[Au_2(dmpm)_2](PF_6)_2$, 68 and 0.27; $[Au_2(dmpm)_3](PF_6)_2$, 69 and 0.28; $[Au_2(dmpm)_2]Cl_2$, 71 and 0.29; $Au_2(dmb)(CN)_2$ (dmb = 1,8-diisocyano-*p*-menthane), 36 and 0.075. Including literature results, data banks of four and eleven points are accumulated for the silver and gold compounds, respectively, where reparametrized Herschbach-Laurie type relationships (H-L) between $r(M_2)$ and $F(M_2)$ applied to Ag_2 or Au_2 systems are designed. For $Ag_2(dmpm)_2Br_2$ ($\nu(Ag_2)$ = 48 cm^{-1}), the estimated $F(Ag_2)$ for the intramolecular Ag···Ag interactions is 0.03 mdyn $Å^{-1}$. Crystallographic details are as follows. For $Ag_2(dmpm)_2Br_2$: monoclinic space group $P2_1/n$, a = 7.2023 (8) Å, b = 10.5734 (5) Å, c = 14.1980 (6) Å, β = 82.466 (9)°, Z = 2, R = 0.040 for 1382 reflections measured. For $[Au_2(dmpm)_2](PF_6)_2$: monoclinic space group $C2/m$, a = 10.234 (1) Å, b = 13.711 (2) Å, c = 9.525 (2) Å, β = 96.74 (1)°, Z = 2, R = 0.050 for 1540 reflections where $F_o^2 > 3\sigma(F_o^2)$.

Introduction

Empirical equations relating atom-atom distances (r) and atom-atom force constants (F),[2,3] or atom-atom stretching frequencies (ν),[4,5] are numerous. The reported equations relating r and F have different mathematical forms going from Badger's ($r = a + b(F^{-1/3})$)[2a] to Herschbach and Laurie's ($r = a + b(\log F)$)[2b] to Woodruff's rules ($r = a + b\exp(-F/c)$).[3] The latest ones have been specifically designed to include systems containing M_2 units for which the M_2 separations were relatively long and have been succesfully used for M_2 complexes (M = Rh, Pd, Pt).[6] In the family of diphosphine M_2 complexes exhibiting long $r(M_2)$ are found the Ag_2 and Au_2 compounds.[7,8] We are interested in these systems, since they exhibit long-lived lowest energy excited states (0.2-2.4 μs) and their photochemical reactivity and photophysical properties depend, in part, upon the M_2 interactions.[8j,9]

Recently we have reported the preparation and characterization of the luminescent compound $Au_2(tmb)Cl_2$ (tmb = 2,5-dimethyl-2',5'-diisocyanohexane), in which no intramolecular Au_2 interactions occur; however, small intermolecular Au···Au contacts ($r(Au_2)$ = 3.3 Å) are observed in the solid state.[10] Indeed, an intense $\nu(Au_2)$ Raman band located at 50 cm^{-1} was assigned, and an associated $F(Au_2)$ of 0.14 mdyn $Å^{-1}$ was reported for these interactions. Also, Che et al.[8j] have published the crystal structure of $Au_2(dmb)(CN)_2$ (dmb = 1,8-diisocyano-*p*-menthane), for which, while the intramolecular Au_2 interaction ($r(Au_2)$ = 3.536 (1) Å) is weak, clear molecular distortions favoring the Au_2 interactions are nonetheless observed. M_2 systems exhibiting very weak M_2 interactions are not uncommon. For instance, $Hg_2(^1\Sigma_g^+)$ and $Hg_2(^1\Sigma_u^+)$ also exhibit long $r(Hg_2)$ and low $\nu(Hg_2)$ ($r(Hg_2)$ = 3.63 ● 0.04 and 3.61 ± 0.05 Å and $\nu(Hg_2)$ = 18.5 ● 0.5 and

* To whom correspondence should be addressed.

(1) (a) Université de Sherbrooke. (b) California Institute of Technology. (c) All correspondance pertaining the crystallography studies should be addressed to these authors.
(2) (a) Badger, R. M. *J. Chem. Phys.* **1934**, *2*, 128; **1935**, *3*, 710. (b) Hershbach, D. R.; Laurie, V. W. *J. Chem. Phys.* **1961**, *35*, 458.
(3) (a) Miskowski, V. M.; Dallinger, R. F.; Christoph, G. G.; Morris, D. E.; Spies, G. H.; Woodruff, W. H. *Inorg. Chem.* **1987**, *26*, 2127. (b) Conradson, S. D.; Sattelberger, A. P.; Woodruff, W. H. *J. Am. Chem. Soc.* **1988**, *110*, 1309. (c) Woodruff, W. H. Unpublished results.
(4) (a) Butler, I. S.; Harvey, P. D.; McCall, J. M.; Shaver, A. *J. Raman Spectrosc.* **1986**, *17*, 221. (b) Steudel, R. *Z. Naturforsch.* **1975**, *30B*, 281.
(5) Codier, C. Ph.D. Thesis, Université Paris VI, 1991.
(6) (a) Harvey, P. D.; Gray, H. B. *J. Am. Chem. Soc.* **1988**, *110*, 4391. (b) Harvey, P. D.; Adar, F.; Gray, H. B. *J. Am. Chem. Soc.* **1989**, *111*, 1312.
(7) (a) Ho, D. M.; Bau, R. *Inorg. Chem.* **1983**, *22*, 4073. (b) Tiekink, E. R. T. *Acta Crystallogr.* **1990**, *C46*, 235. (c) Karsh, H. H.; Schubert, U. *Z. Naturforsch.* **1982**, *B37*, 186.
(8) (a) Schmidbaur, H.; Pollok, Th.; Herr, R.; Wagner, F. E.; Bau, R.; Riede, J.; Müller, G. *Organometallics* **1986**, *5*, 566. (b) Schmidbaur, H.; Wohlleben, A.; Schubert, U.; Frank, A.; Huttner, G. *Chem. Ber.* **1977**, *110*, 2751. (c) Schmidbaur, H.; Mandl, J. R.; Bassett, J.-M.; Blaschke, G.; Zimmer-Gasser, B. *Chem. Ber.* **1981**, *114*, 433. (d) Briant, C. E.; Hall, K. P.; Mingos, D. M. P. *J. Organomet. Chem.* **1982**, *229*, C5. (e) Kozelka, J.; Oswald, H. R.; Dubler, E. *Acta Crystallogr.* **1986**, *C42*, 1007. (f) Bensch, W.; Prelati, M.; Ludwig, W. *J. Chem. Soc., Chem. Commun.* **1986**, 1762. (g) Payne, N. C.; Puddephatt, R. J.; Ravindranath, R.; Treunicht, I. *Can. J. Chem.* **1988**, *66*, 3176. (h) Jaw, H.-R. C.; Savas, M. M.; Rodgers, R. D.; Mason, W. R. *Inorg. Chem.* **1989**, *28*, 1028. (i) Khan, Md. N. I.; King, C.; Heinrich, D. D.; Fackler, J. P., Jr.; Porter, L. C. *Inorg. Chem.* **1989**, *28*, 2150. (j) Che, C.-M.; Wong, W.-T.; Lai, T.-F.; Kwong, H.-L. *J. Chem. Soc., Chem. Commun.* **1989**, 243.

0020-1669/92/1331-0695$03.00/0